SCIENCE CHINA
Chemistry

• ARTICLES •
· SPECIAL TOPIC · Frontiers in Polymer Science

doi: 10.1007/s11426-016-0198-0

# Realizing 11.3% efficiency in fullerene-free polymer solar cells by device optimization

Wenchao Zhao[1,2], Shaoqing Zhang[1] & Jianhui Hou[1,2*]

[1]*State Key Laboratory of Polymer Physics and Chemistry; Beijing National Laboratory for Molecular Sciences, Institute of Chemistry, Chinese Academy of Sciences, Beijing 100190, China*
[2]*University of Chinese Academy of Sciences, Beijing 100049, China*

Received April 29, 2016; accepted May 25, 2016

In this work, photovoltaic properties of the PBDB-T:ITIC based-NF-PSCs were fully optimized and characterized by tuning the morphology of the active layers and changing the device architecture. First, donor/acceptor (D/A) weight ratios were scanned, and then further optimization was performed by using different additives, i.e. 1,8-diiodooctane (DIO), diphenyl ether (DPE), 1-chloronaphthalene (CN) and *N*-methyl-2-pyrrolidone (NMP), on the basis of best D/A ratio (1:1, *w*/*w*), respectively. Finally, the conventional or inverted device architectures with different buffer layers were employed to fabricate NF-PSC devices, and meanwhile, the morphology of the active layers was further optimized by controlling annealing temperature and time. As a result, a record efficiency of 11.3% was achieved, which is the highest result for NF-PSCs. It's also remarkable that the inverted NF-PSCs exhibited long-term stability, i.e. the best-performing devices maintain 83% of their initial PCEs after over 4000 h storage.

**polymer solar cells, morphology, interfacial layers, device architecture, stability**

**Citation:** Zhao W, Zhang S, Hou J. Realizing 11.3% efficiency in fullerene-free polymer solar cells by device optimization. *Sci China Chem*, 2016, 59: 1–9, doi: 10.1007/s11426-016-0198-0

## 1 Introduction

Bulk heterojunction (BHJ) polymer solar cells (PSCs), consisting of a p-type semiconducting polymer as the electron donor and a fullerene derivative as the electron acceptor have received considerable attention for years [1−5]. Enormous research efforts, such as designing and synthesizing novel materials, developing novel processing methods in device engineering, and investigating electrode buffer layers, have been made in the PSCs field, and the power conversion efficiencies (PCEs) of PSCs have been improved from 1% to 10% in recent publications [6−14]. Although fullerene derivatives have been widely applied as electron acceptor in the PSCs and achieved great progress, they still have several drawbacks such as weak light absorption in the visible region and high production costs [15]. In recent years, various non-fullerene acceptors including rylene-based materials and indacenodithiophene-based acceptors have been developed and applied in PSCs [16−19]. Indaceno [1,2-b:5,6-b′] dithiophene (IDT)-based acceptors are the best acceptors at this moment. Zhan group [20,21] reported a series of non-fullerene acceptors and is the pioneer in this field in the world [22,23]. However, PCEs of non-fullerene-based polymer solar cells (NF-PSCs) have lagged behind fullerene-based PSCs [24−34]. Therefore, how to promote the PCEs of NF-PSCs is still an interesting and important topic in the field of PSCs.

By now, varied methods were developed to improve the photovoltaic performance of the NF-PSCs.

*Corresponding author (email: hjhzlz@iccas.ac.cn)

Among them, developing novel non-fullerene materials and optimizing device fabrication methods are very helpful to achieve high PCEs [24−33]. For example, Zhan *et al.* [21] explored a novel NF-acceptors, 3,9-bis(2-methylene-(3-(1,1-dicyanomethylene)-indanone)-5,5,11,11-tetrakis(4-hexylphenyl)-dithieno[2,3-d:2′,3′-d′]-s-indaceno[1,2-b:5,6-b′]dithiophene (ITIC), with superior properties, such as good electron transport ability and miscibility with polymer donors. A newly developed polymer poly[[2,6′-4,8-di(5-ethylhexylthienyl)benzo[1,2-b;3,3-b] dithiophene][3-fluoro-2[(2-ethylhexyl)carbonyl]thieno[3,4-b]thiophenediyl]] (PTB7-Th) was selected as the donor material to match with ITIC, and a promising PCE of 6.8% was achieved. In 2016, Wang and coworkers [27] reported a new NF-acceptor, SdiPBI-Se, and optimized photovoltaic properties of the PSC devices based on the blend of SdiPBI-Se and a donor polymer poly[dithieno[2,3-d:2′,3′-d′]benzo[1,2-b:4,5-b′]dithiophene-co-1,3-bis(thiophen-2-yl)-benzo-[1,2-c:4,5-c′]dithiophene-4,8-dione] (PDBT-T1) by using chlorobenzene (CB) as the host solvent and 0.25% 1,8-diiodooctane (DIO) as the additive, and obtained a PCE of 8.43%. Recently, Li *et al.* [29] used a medium bandgap 2D-conjugated polymer donor materials J61 with ITIC to make devices and achieved a PCE of 9.53% by thermal annealing under 100 °C for 10 min and also adopting a conventional device architecture with PDINO (a perylene diimides functionalized with amino *N*-oxide) as cathode buffer layer. On the basis of the reported works, we can find that in order to get high PCE in NF-PSCs, several factors should be taken into consideration, i.e. the active layer composition, the device processing methods, the interfacial layer and the device architecture [35]. Very recently, we utilized a 2D-conjugated polymer poly[(2,6-(4,8-bis(5-(2-ethylhexyl)thiophen-2-yl)benzo[1,2-b:4,5-b′]dithiophene)-co-(1,3-di(5-thiophene-2-yl)-5,7-bis(2-ethylhexyl)benzo[1,2-c:4,5-c′]dithiophene-4,8-dione)] (PBDB-T) [36] as donor and ITIC [21] as acceptor to fabricate PSC devices and realized a high PCE of 11.21% [37]. However, the detailed device optimization process and the device photovoltaic properties under different fabrication conditions have not been discussed yet. In this work, the device optimization process of NF-PSCs based on PBDB-T:ITIC was provided in detail, and the influences of varied processing methods on device performance were discussed. What is more, the stability of the device prepared under the optimal conditions was provided and discussed.

## 2 Experimental

### 2.1 Materials

5,7-Bis(2-ethylhexyl)benzo [1,2-c:4,5-c′] dithiophene-4,8-dione (PBDB-T, Figure 1), the number average molecular weight ($M_n$) of PBDB-T was 29 kDa with a polydispersity index (PDI) of 1.5. PBDB-T and hydrochloric acid doped polyanilines (HAPAN) were synthesized in our laboratory according to our previous works [36,38]. Poly[(9,9-dioctyl-2,7-fluorene)-alt-(9,9-bis(3′-(*N*,*N*-dimethylamino)propyl)-2,7-fluorene)] PFN and ITIC (Figure 1) was purchased from Solarmer Materials (Beijing) Inc, China. The processing solvents used in the device fabrication processes were purchased from Alfa Aesar, USA. The ZnO solution was synthesized according to the literature [26]. Poly(3,4-ethylenedioxythiophene) poly(styrenesulfonate) (PEDOT:PSS) (AI 4083) and electrode materials were commercially available products without further purification.

### 2.2 Device fabrication

The conventional PSCs with a device architecture of ITO/PEDOT:PSS (HAPAN)/BHJ blend/Ca/Al and the inverted PSCs with a device architecture of ITO/ZnO (PFN)/BHJ blend/$MoO_3$/Al were prepared (Figure 1). ITO substrates with a sheet resistance of 15 Ω/sq were cleaned with detergent water, deionized water, acetone and isopropyl alcohol in an ultrasonic bath sequentially for 20 min, and then dried in an oven at 150 °C for 30 min. The PEDOT:PSS solution should be filtered by a Nylon filter with a diameter of 0.45 μm prior to the spin cast. The concentration of PBDB-T:ITIC (1:1, *w*/*w*) in CB solution is 10 mg/mL for the polymer. The thickness of PBDB-T:ITIC blend film was ~100 nm. The conventional device was deposited by thermal evaporation of Ca (10 nm) and then Al (100 nm), and the inverted device was completed by thermal evaporation of $MoO_3$ (10 nm) and Al (100 nm) through a mask with a 4 $mm^2$ active area under vacuum at a pressure of $3\times10^{-4}$ Pa.

### 2.3 Instruments and measurements

Current density-voltage (*J*-*V*) characteristics were measured under the 100 $mW/cm^2$ standard AM 1.5G spectrum using a solar simulator (AAA grade). The simulator was calibrated by a NIM certificated silicon solar cell (KG3 color filter, China). The external quantum efficiency (EQE) data

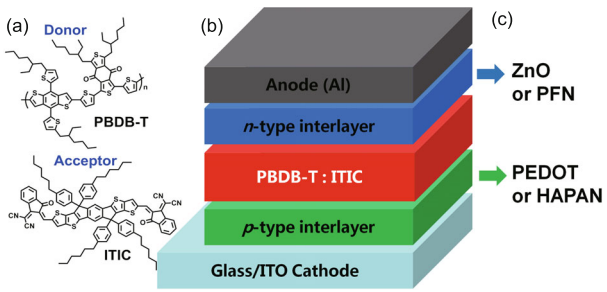


**Figure 1** Molecular structures of polymer donor (PBDB-T) and non-fullerene acceptor (ITIC) (a) and device diagram of PSCs (b) with various buffer layer (c) (color online).

were collected by an integrated IPCE measurement system, namely QE-R3011 (Enli Technology Co. Ltd., Taiwan, China). The surface topography and phase images of thin film were obtained using the atomic force microscopy (AFM) in topping mode. The thickness of the BHJ blend films were measured by a Bruker Dektak XT profilometer (Germany).

## 3 Results and discussion

### 3.1 Photovoltaic properties and morphological characteristics with varied donor/acceptor (D/A) ratio

#### 3.1.1 Photovoltaic properties with varied D/A ratio

Initially, the NF-PSCs devices were fabricated to obtain the optimal D/A ratio of PBDB-T:ITIC blend film with the conventional structure using PEDOT:PSS as anode buffer layer, and CB was used to prepare the solutions for spin-coating of the active layers. The current density-voltage (*J-V*) curves of the conventional PSC devices under the illumination of AM 1.5 G, 100 mW/cm$^2$ are shown in Figure 2(a), and the corresponding EQE spectra are shown in Figure 2(b). The photovoltaic parameters are collected in Table 1. The blended film at D/A weight ratio of 1:1 gave the best PCE of 8.62% with an open circuit voltage ($V_{oc}$) of 0.89 V, a short circuit current density ($J_{sc}$) of 15.13 mA/cm$^2$, and a fill factor (*FF*) of 0.64. The best PCE data were acquired with the thickness at ~100 nm (Table 1). The EQE spectrum of PBDB-T:ITIC devices (1:1) has two peaks of ca. 67% in the region of 550−700 nm.

#### 3.1.2 Morphological study with varied D/A ratio

Understanding the morphology and phase separation is a key to further improvement of PSC performance, thus it is of great importance to learn the morphological properties and the interactions in the blend films [39,40]. The morphologies of the PBDB-T:ITIC blend films with different D/A ratios were investigated using AFM, and the height and phase images (2 μm×2 μm) are shown in Figure 3. As shown, we can see that (1) PBDB-T and ITIC have good miscibility with varied D/A ratios (from 1.3:1 to 1:1.5); (2) it can be observed that the mean square surface roughnesses ($R_q$) value of the blend film with D/A ratio of 1:1 (2.97 nm) is considerable value with 1.3:1 (3.48 nm) and 1:1.3 (3.53 nm) D/A ratio, but smaller than 1:1.5 (6.18 nm) D/A ratio due to the pure ITIC film shows a rougher surface with $R_q$=5.46 nm [37]. The low *FF* observed in the PSCs devices with the D/A ratio with 1.3:1; 1:1.3 and 1:1.5 might be attributed to the morphology of large-scale phase separation.

### 3.2 Photovoltaic properties and morphological characteristics with varied additives

#### 3.2.1 Photovoltaic properties with varied additives

The effects of processing solvent additives such as DIO, diphenyl ether (DPE), 1-chloronaphthalene (CN) and *N*-methyl-2-pyrrolidone (NMP) on device performance have been well studied in PCBM-based PSCs [41−44]. In this work, on the basis of 1:1 D/A ratio, different solvent additives with varied volume ratios were used to optimize active layer morphology and thus to further improve device performance of the NF-PSCs, and the molecular structures of the additives were shown in Figure 4. The corresponding *J-V* curves of the NF-PSCs fabricated with varied solvent additives are illustrated in Figure 5 and the detailed photovoltaic parameters are summarized in Table 2. For the devices prepared by using CB with varied amount of DIO, when 0.5% DIO was used as the additive, a high PCE of 9.93% can be achieved with $V_{oc}$ of 0.898 V, $J_{sc}$ of 16.90 mA/cm$^2$ and *FF* of 0.654. The photovoltaic parameters of the devices are very similar as those in our recent work [37]. Besides of DIO, other additives such as DPE, CN and NMP were used to fabricated PSC devices. As shown in Figure 5 and Table 2, when 1% DPE, 1% CN and 1% NMP were mixed with CB for making the solutions of PBDB-T and ITIC, the PCEs of 9.35%, 9.16% and 9.23% can be achieved, respectively, which is lower than that of the device fabricated by with 0.5% DIO. To understand the differences of photovoltaic performance of the above-mentioned NF-PSCs, photocurrent behavior

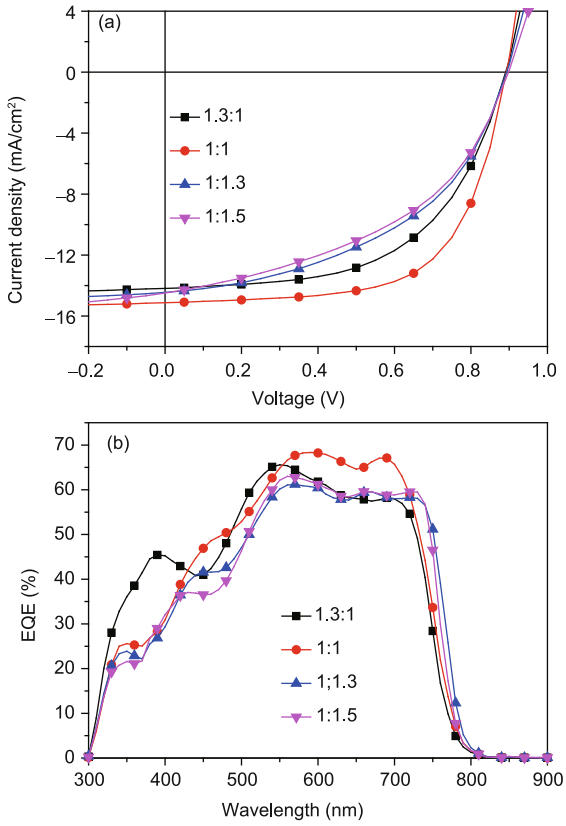


**Figure 2** (a) *J-V* of the NF-PSCs based on varied D/A ratio under the illumination of AM 1.5G 100 mW/cm$^2$; (b) EQE curve of the corresponding device (color online).

**Table 1** Photovoltaic properties of the NF-PSCs based on structure of ITO/PEDOT:PSS/ PBDB-T:ITIC/Ca/Al without additive under the illumination of AM 1.5 G, 100 mW/cm$^2$

| D/A | $V_{oc}$ (V) | $J_{sc}$ (mA/cm$^2$) | *FF* | PCE [a] (%) | PCE$_{max}$ (%) | Thickness (nm) |
|---|---|---|---|---|---|---|
| 1.3:1 | 0.89 | 14.19 | 0.56 | 6.84±0.15 | 7.07 | 100 |
| 1:1 | 0.89 | 15.13 | 0.64 | 8.27±0.19 | 8.62 | |
| 1:1.3 | 0.89 | 14.44 | 0.48 | 5.88±0.18 | 6.17 | |
| 1:1.5 | 0.90 | 14.49 | 0.45 | 5.64±0.20 | 5.87 | |

a) Average value from 10 individual devices.

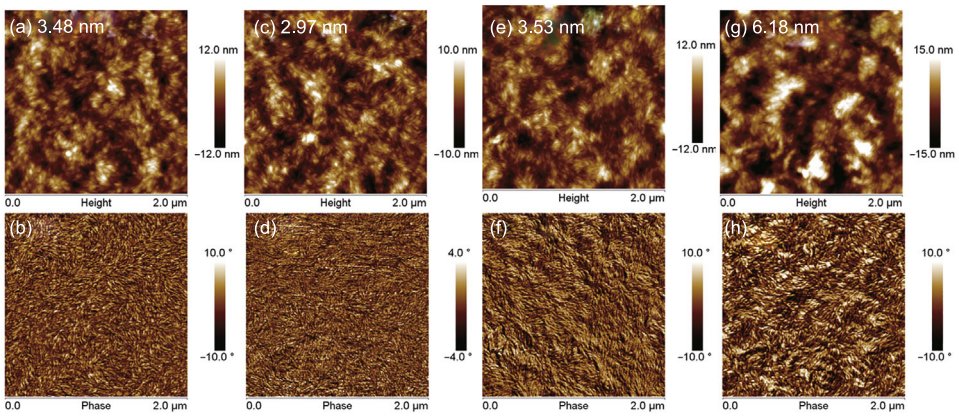


**Figure 3** The AFM height and phase images of PBDB-T:ITIC blend films with D/A ratios of 1.3:1 (a, b), 1:1 (c, d), 1:1.3 (e, f) and 1:1.5 (g, h), respectively (color online).

**Table 2** Photovoltaic properties of the NF-PSCs processed by CB and varied amount of DIO, DPE, CN and NMP under the illumination of AM 1.5G 100 mW/cm$^2$, respectively

| Additive | $V_{oc}$ (V) | $J_{sc}$ (mA/cm$^2$) | *FF* | PCE [a] (%) | PCE$_{max}$ (%) |
|---|---|---|---|---|---|
| 0.5% DIO | 0.898 | 16.90 | 0.654 | 9.72±0.16 | 9.93 |
| 1.0% DIO | 0.892 | 16.47 | 0.613 | 8.75±0.19 | 9.01 |
| 3.0% DIO | 0.894 | 16.27 | 0.582 | 8.18±0.23 | 8.47 |
| 0.5% DPE | 0.889 | 16.64 | 0.600 | 8.52±0.25 | 8.88 |
| 1.0% DPE | 0.900 | 16.84 | 0.617 | 9.10±0.18 | 9.35 |
| 3.0% DPE | 0.893 | 16.21 | 0.621 | 8.71±0.28 | 8.99 |
| 0.5% CN | 0.910 | 15.35 | 0.634 | 8.51±0.28 | 8.86 |
| 1.0% CN | 0.914 | 15.21 | 0.659 | 8.90±0.20 | 9.16 |
| 3.0% CN | 0.897 | 14.87 | 0.633 | 8.19±0.22 | 8.44 |
| 0.5% NMP | 0.885 | 16.25 | 0.633 | 8.82±0.21 | 9.10 |
| 1.0% NMP | 0.889 | 16.22 | 0.640 | 9.02±0.19 | 9.23 |
| 3.0% NMP | 0.880 | 15.97 | 0.622 | 8.50±0.20 | 8.74 |

a) Average value from 10 individual devices.

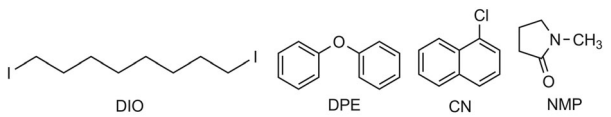


**Figure 4** Molecular structures of DIO, DPE, CN and NMP.

analysis was carried out according to the literature [45]. As shown in Figure 6, a high exciton dissociation probability ($P_{ed}$) of 92.5% was achieved based on device processed with DIO under short circuit condition, the exciton dissociation efficiency of the device processed with DIO is slightly higher than the devices processed with the other additives, which contributes to the higher $J_{sc}$ and *FF* of the NF-PSC processed with CB/0.5% DIO.

### 3.2.2 Morphological study with varied additives

The topography and surface roughness of PBDB-T:ITIC blend films with various solvent additives were studied using AFM. As displayed in Figure 7, when 0.5% DIO was used as solvent additive, the corresponding PBDB-T:ITIC blend film shows a smooth surface with a $R_q$ of 2.21 nm and weaker aggregation effect. In comparison, the blend film processed with CB/1% DPE, CB/1% CN and CB/1% NMP have rougher surfaces with larger phase-separated domains. The surface morphologies revealed the blend film processed by the mixture CB and 0.5% DIO shows a smoother surface

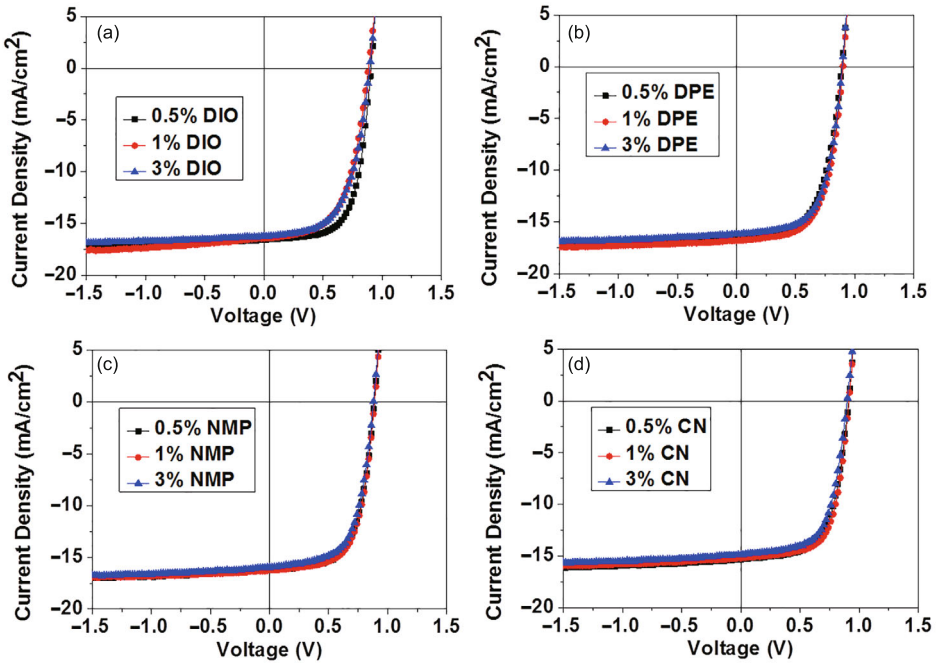


**Figure 5** *J-V* curves of the NF-PSCs processed by CB and varied amount of DIO (a), DPE (b), CN (c) and NMP (d) under the illumination of AM 1.5 G 100 mW/cm$^2$, respectively (color online).

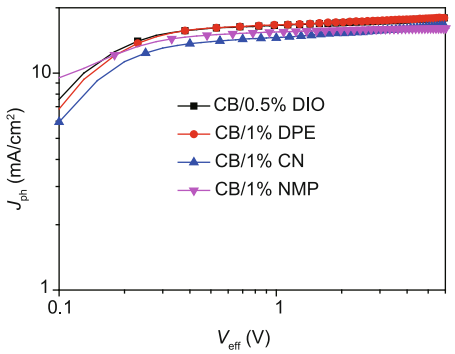


**Figure 6** Photocurrent versus effective voltage plots of NF-PSCs fabricated with CB/0.5% DIO, CB/1% DPE, CB/1% CN and CB/1% NMP (color online).

with small size aggregations, which could be the reason for the better $J_{sc}$ and *FF* of the corresponding device.

### 3.3 Photovoltaic properties with the NF-PSCs with different devices structures

Interfacial buffer layers have played a vital role in promoting photovoltaic performance of NF-PSCs [26,31,35]. Many types of interfacial buffer layers have been successfully employed in high-performance NF-PSCs to facilitate charge carrier collection from active layer to electrodes. Recently, our group [38] reported an anode buffer layer of HAPAN which exhibits superior properties. Here, we select HAPAN as anode buffer layer to replace the function of PEDOT:PSS in the conventional device architecture. The energy levels and work functions of the materials involved in this work are provided in Figure 8. *J-V* curves of the NF-PSCs with both PEDOT:PSS and HAPAN as anode buffer layer are shown in Figure 9(a), and the device performance parameters are summarized in Table 3. The devices based on HAPAN as anode buffer layer exhibited comparable photovoltaic performance with the devices using PEDOT:PSS. As clearly seen in the dark *J-V* curves (Figure 9(b)), a relatively low leakage current and a high rectification ratio was recorded in the device with PEDOT:PSS.

Then, the NF-PSCs with inverted architecture were fabricated to further improve the PCEs. Here, we utilized two solution processed interlayer materials, ZnO and PFN, to modify the ITO electrodes according to the reported works [26,31]. As well-known, thermal annealing has been employed to manipulate the morphologies of the active layers in many photovoltaic systems including P3HT/PCBM [46] and other polymer/non-fulleren acceptor blends [47]. Therefore, thermal annealing treatment was also applied to improve device performance in this work. The PBDB-T:ITIC-based devices were fabricated under different annealing temperatures with an inverted configuration of ITO/ZnO/PBDB-T:ITIC/$MoO_3$/Al. The photovoltaic results ($V_{oc}$, $J_{sc}$, *FF* and PCE) of NF-PSCs based on PBDB-T:ITIC with different annealing temperature are shown in Figure 10. An excellent PCE of 11.3% was achieved with a $J_{sc}$ of 17.20 mA/cm$^2$, a $V_{oc}$ of 0.90 V, and a *FF* of 0.73 under 160 °C for 30 min. Meanwhile, for the PBDB-T:ITIC based PSCs

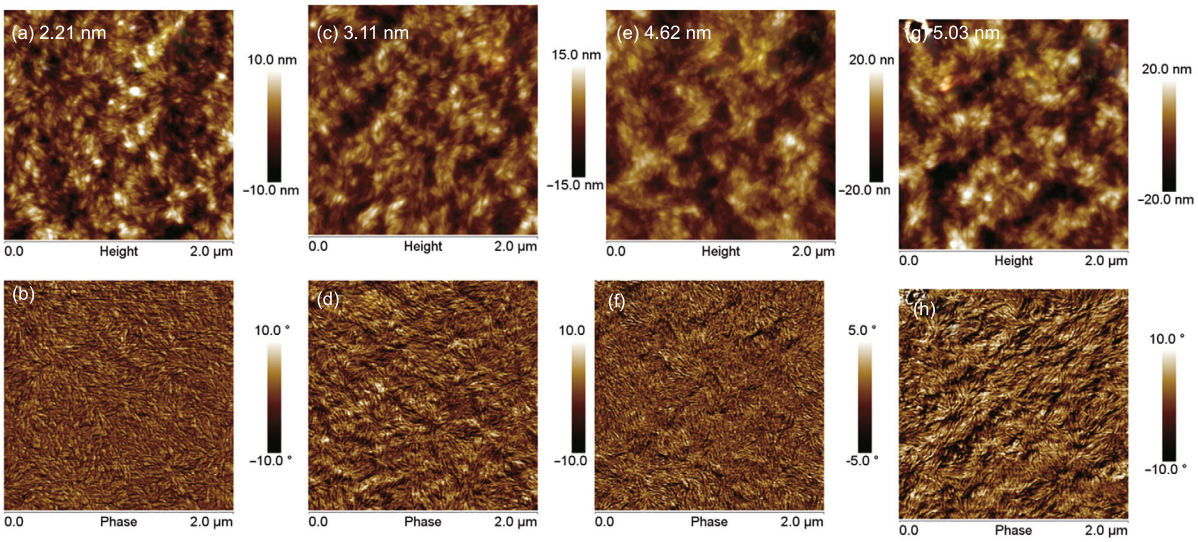


**Figure 7** AFM height and phase images of the blend films of PBDB-T:ITIC processed with CB/0.5% DIO (a, b), CB/1% DPE (c, d), CB/1% CN (e, f) and CB/1% NMP (g, h), respectively (color online).

**Table 3** Photovoltaic properties of the NF-PSCs based on PBDB-T:ITIC with various anode buffer layer

| Interlayer | $V_{oc}$ (V) | $J_{sc}$ (mA/cm$^2$) | *FF* | PCE [a] (%) | $PCE_{max}$ (%) |
|---|---|---|---|---|---|
| PEDOT:PSS | 0.898 | 16.90 | 0.654 | 9.72±0.16 | 9.93 |
| HAPAN | 0.902 | 16.61 | 0.649 | 9.51±0.19 | 9.72 |

a) Average value from 10 individual devices.

**Table 4** Photovoltaic properties of NF-PSCs based on PBDB-T:ITIC with ZnO and PFN as cathode buffer layer

| Interlayer | $V_{oc}$ (V) | $J_{sc}$ (mA/cm$^2$) | *FF* | PCE [a] (%) | $PCE_{max}$ (%) |
|---|---|---|---|---|---|
| ZnO | 0.90 | 17.20 | 0.73 | 10.71±0.24 | 11.30 |
| PFN | 0.89 | 17.05 | 0.71 | 10.35±0.28 | 10.77 |
| ZnO [b] | 0.91 | 17.30 | 0.69 | | 10.9 |

a) Average value from 10 individual devices; b) the photovoltaic data collected from the test report provided by National Institute of Metrology, China.

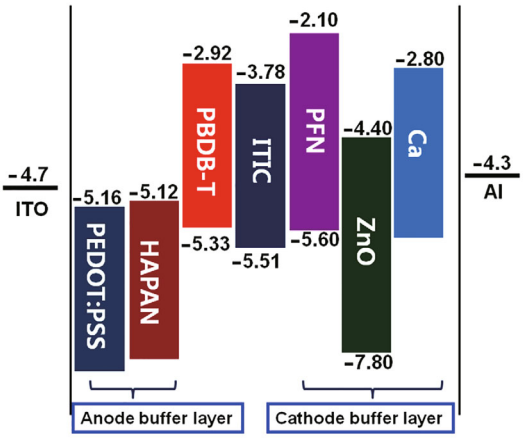


**Figure 8** Energy level diagram of NF-PSCs based on PBDB-T:ITIC with various electrode buffer layer (color online).

with the inverted architecture were fabricated with PFN as cathode buffer layer, as shown in Figure 11(a) and Table 4, a high PCE of approximately 11% were obtained. The devices with ZnO as interlayer show slightly higher EQE than the device with PFN as interlayer (Figure 11(b)). The statistical data were listed in Table 4, and both two types of the inverted devices show reproducible high photovoltaic performance with small standard deviations.

### 3.4 Certification of the NF-PSCs based on PBDB-T:ITIC

In order to get reliable photovoltaic results, we provided the certifications for photovoltaic measurements of PSCs [48]. As reported in our previous work, a NF-PSC with 1.00-cm$^2$ area was fabricated and sent to Enli Tech Optoelectronic Calibration Lab for certification. A rated efficiency of 10.78% was obtained, and to the best of our knowledge, this is the highest value recorded of the PSCs with single junction structure with an area of 1.00-cm$^2$ [37]. Herein, the devices with the structure of ITO/ZnO/PBDB-T:ITIC/$MoO_3$/Al were fabricated under the optimal conditions and the photovoltaic properties were certified by National Institute of Metrology (NIM), China. The *J-V* curves and photovoltaic parameters obtained from the certification report are shown in

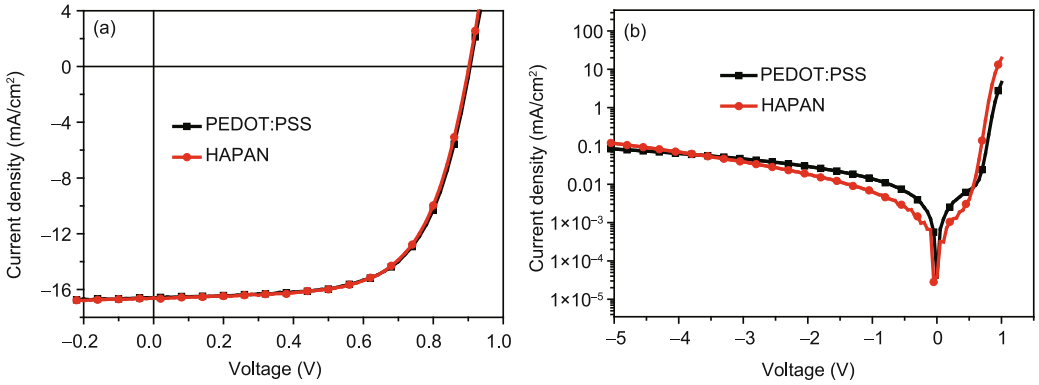


**Figure 9** The *J-V* curves in the light (a) and in the dark (b) of conventional PSCs based on PBDB-T:ITIC with various anode buffer layer (color online).

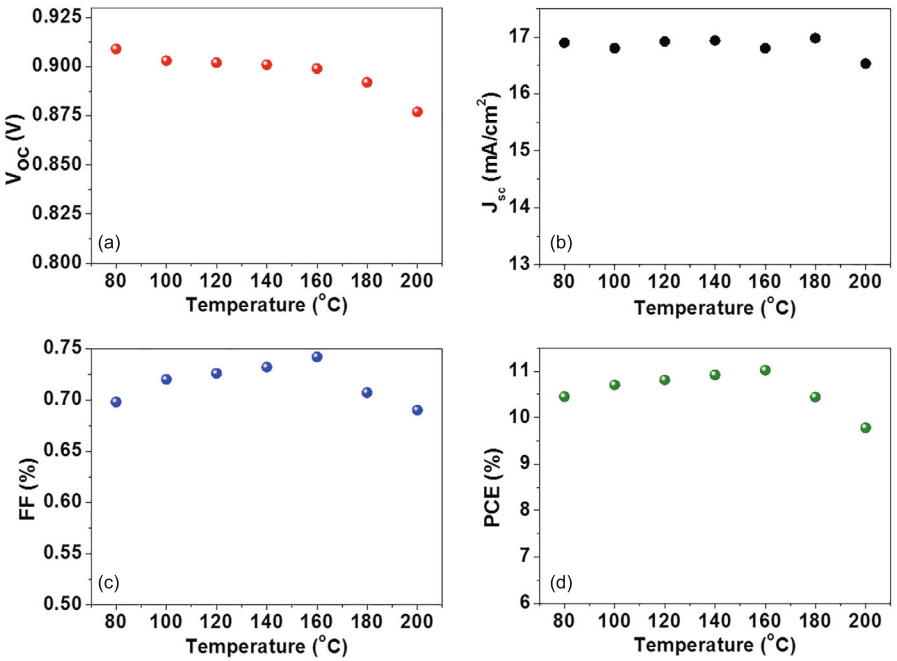


**Figure 10** Effect of the annealing temperature on the $V_{oc}$ (a), $J_{sc}$ (b), *FF* (c) and PCE (d) of the PBDB-T:ITIC based NF-PSCs.

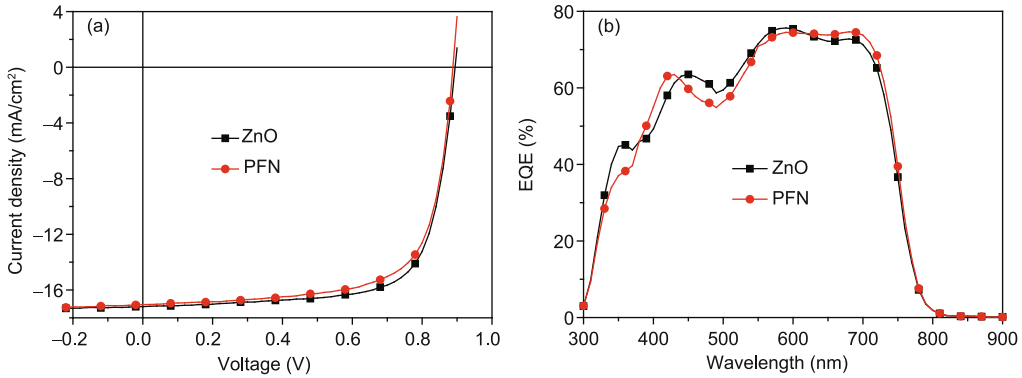


**Figure 11** The *J-V* curves (a) and EQE spectra (b) of inverted PSCs with various cathode buffer layer based on PBDB-T:ITIC.

Figure 12 and Table 4 (certificate number of the report is GXtc2015-1823). The certificated PCE is 10.9%, which is very similar to the result obtained in our laboratory (11.3%), indicating our inner results are reliable. Long-term dev-

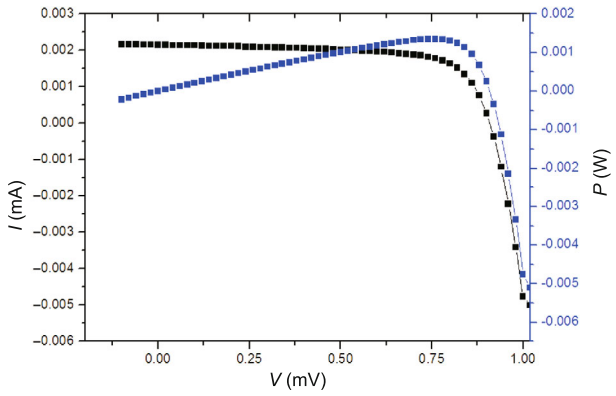


**Figure 12** Certificate report of the PBDB-T:ITIC based NF-PSCs by National Institute of Metrology, China (color online).

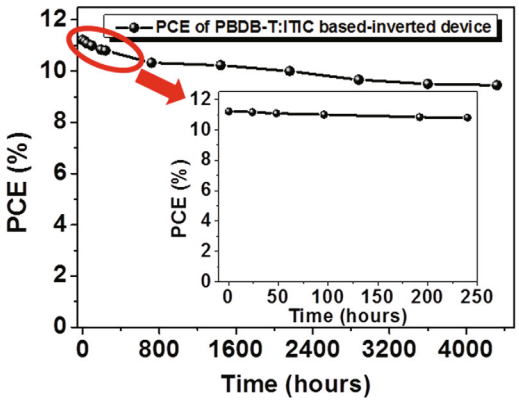


**Figure 13** The long-term stability of PBDB-T:ITIC based-inverted PSC devices which were stored in $N_2$ filled glove box (color online).

ice stability of PSCs is one of the critical issues for practical applications [49,50]. Figure 13 shows the long-term stability of an inverted NF-PSC based on PBDB-T:ITIC in $N_2$ filled glove box. The device can achieve 9.32% with a $J_{sc}$ of 15.91 mA/cm$^2$, a $V_{oc}$ of 0.885 V, and a *FF* of 0.662 after over 4000 h storage, which is only 16.86% degradation compared to the original PCE (11.21%). Meanwhile, Encapsulated NF-PSCs have been exposed to continuous illumination with AM 1.5G illumination, the PCE is no significant degradation after 6 h, and then encapsulated fullerene-free PSCs was annealed with 100 °C for 2 h, the NF-PSCs maintained 80% of their initial PCEs. All these results demonstrate that inverted NF-PSCs based on PBDB-T:ITIC blend film have good stabilities.

## 4 Conclusions

In conclusion, we demonstrate that high-performance of NF-PSCs can be achieved, step by step, by optimizing the device fabrication process in detail such as selecting the appropriate D/A weight ratio, changing the processing additives (DIO, DPE, CN and NMP), thermal annealing to manipulate the morphology of active layer and employing conventional or inverted device architecture with different interlayer materials. As a result, a promising PCE of 11.3% was achieved in the PBDB-T:ITIC based device, which is the highest result reported so far for NF-PSCs. Other than that, the inverted NF-PSCs exhibited long-term stability and maintained 83% of their initial PCEs after over 4000 h storage. These results demonstrate the detailed optimization procedures of the high performance PBDB-T:ITIC-based PSCs and can be used as a guideline for device fabrication of NF-PSCs.

**Acknowledgments** This work was supported by the National Basic Research Program (2014CB643501), the National Natural Science Foundation of China (91333204, 21325419), and the Chinese Academy of Sciences (XDB12030200)

**Conflict of interest** The authors declare that they have no conflict of interest.

1 Halls JJM, Walsh CA, Greenham NC, Marseglia EA, Friend RH, Moratti SC, Holmes AB. *Nature*, 1995, 376: 498–500
2 Yu G, Gao J, Hummelen JC, Wudl F, Heeger AJ. *Science*, 1995, 270: 1789–1791
3 Li Y. *Acc Chem Res*, 2012, 45: 723–733
4 Ye L, Zhang S, Huo L, Zhang M, Hou J. *Acc Chem Res*, 2014, 47: 1595–1603
5 Duan C, Huang F, Cao Y. *J Mater Chem*, 2012, 22: 10416–10434
6 Zhang S, Ye L, Hou J. *Adv Energy Mater*, 2016, 6: 1502529
7 Zhang ZG, Li Y. *Sci China Chem*, 2015, 58: 192–209
8 You J, Dou L, Yoshimura K, Kato T, Ohya K, Moriarty T, Emery K, Chen CC, Gao J, Li G, Yang Y. *Nat Commun*, 2013, 4: 1446
9 He Z, Xiao B, Liu F, Wu H, Yang Y, Xiao S, Wang C, Russell TP, Cao Y. *Nat Photon*, 2015, 9: 174–179
10 Liu Y, Zhao J, Li Z, Mu C, Ma W, Hu H, Jiang K, Lin H, Ade H, Yan H. *Nat Commun*, 2014, 5: 5293
11 Chen JD, Cui C, Li YQ, Zhou L, Ou QD, Li C, Li Y, Tang JX. *Adv Mater*, 2015, 27: 1035–1041
12 Ye L, Zhang S, Zhao W, Yao H, Hou J. *Chem Mater*, 2014, 26: 3603–3605
13 Zhang S, Ye L, Zhao W, Yang B, Wang Q, Hou J. *Sci China Chem*, 2015, 58: 248–256
14 Zhao W, Ye L, Zhang S, Sun M, Hou J. *J Mater Chem A*, 2015, 3: 12723–12729
15 Lin Y, Zhan X. *Mater Horiz*, 2014, 1: 470–488
16 Lin Y, Zhan X. *Adv Energy Mater*, 2015, 5: 1501063
17 Lin Y, Zhan X. *Acc Chem Res*, 2016, 49: 175–183
18 Zhan X, Tan Z, Domercq B, An Z, Zhang X, Barlow S, Li Y, Zhu D, Kippelen B, Marder SR. *J Am Chem Soc*, 2007, 129: 7246–7247
19 Lin Y, Wang Y, Wang J, Hou J, Li Y, Zhu D, Zhan X. *Adv Mater*, 2014, 26: 5137–5142
20 Lin Y, Zhang ZG, Bai H, Wang J, Yao Y, Li Y, Zhu D, Zhan X. *Energy Environ Sci*, 2015, 8: 610–616
21 Lin Y, Wang J, Zhang ZG, Bai H, Li Y, Zhu D, Zhan X. *Adv Mater*, 2015, 27: 1170–1174
22 Lin Y, He Q, Zhao F, Huo L, Mai J, Lu X, Su CJ, Li T, Wang J, Zhu J, Sun Y, Wang C, Zhan X. *J Am Chem Soc*, 2016, 138: 2973–2976
23 Lin Y, Zhao F, He Q, Huo L, Wu Y, Parker TC, Ma W, Sun Y, Wang C, Zhu D, Heeger AJ, Marder SR, Zhan X. *J Am Chem Soc*, 2016, 138:

4955–4961
24 Cheng P, Ye L, Zhao X, Hou J, Li Y, Zhan X. *Energy Environ Sci*, 2014, 7: 1351–1356
25 Ye L, Jiao X, Zhou M, Zhang S, Yao H, Zhao W, Xia A, Ade H, Hou J. *Adv Mater*, 2015, 27: 6046–6054
26 Li S, Zhang H, Zhao W, Ye L, Yao H, Yang B, Zhang S, Hou J. *Adv Energy Mater*, 2016, 6: 1501991
27 Meng D, Sun D, Zhong C, Liu T, Fan B, Huo L, Li Y, Jiang W, Choi H, Kim T, Kim JY, Sun Y, Wang Z, Heeger AJ. *J Am Chem Soc*, 2016, 138: 375–380
28 Lin H, Chen S, Li Z, Lai JYL, Yang G, Mcafee T, Jiang K, Li Y, Liu Y, Hu H, Zhao J, Ma W, Ade H, Yan H. *Adv Mater*, 2015, 27: 7299–7304
29 Gao L, Zhang ZG, Xue L, Min J, Zhang J, Wei Z, Li Y. *Adv Mater*, 2016, 28: 1884–1890
30 Ye L, Sun K, Jiang W, Zhang S, Zhao W, Yao H, Wang Z, Hou J. *ACS Appl Mater Interf*, 2015, 7: 9274–9280
31 Zang Y, Li CZ, Chueh CC, Williams ST, Jiang W, Wang ZH, Yu JS, Jen AKY. *Adv Mater*, 2014, 26: 5708–5714
32 Lin Y, Zhang ZG, Bai H, Wang J, Yao Y, Li Y, Zhu D, Zhan X. *Energy Environ Sci*, 2015, 8: 610–616
33 Zhou Y, Kurosawa T, Ma W, Guo Y, Fang L, Vandewal K, Diao Y, Wang C, Yan Q, Reinspach J, Mei J, Appleton AL, Koleilat GI, Gao Y, Mannsfeld SCB, Salleo A, Ade H, Zhao D, Bao Z. *Adv Mater*, 2014, 26: 3767–3772
34 Zhang S, Qin Y, Uddin MA, Jang B, Zhao W, Liu D, Woo HY, Hou J. *Macromolecules*, 2016, 49: 2993–3000
35 Zhao W, Ye L, Zhang S, Yao H, Sun M, Hou J. *J Phys Chem C*, 2015, 119: 27322–27329
36 Qian D, Ye L, Zhang M, Liang Y, Li L, Huang Y, Guo X, Zhang S, Tan Z, Hou J. *Macromolecules*, 2012, 45: 9611–9617
37 Zhao W, Qian D, Zhang S, Li S, Inganäs O, Gao F, Hou J. *Adv Mater*, 2016, 28: 4734–4739
38 Zhao W, Ye L, Zhang S, Fan B, Sun M, Hou J. *Sci Rep*, 2014, 4: 6570
39 Huang Y, Kramer EJ, Heeger AJ, Bazan GC. *Chem Rev*, 2014, 114: 7006–7043
40 Duan C, Cai W, Hsu BBY, Zhong C, Zhang K, Liu C, Hu Z, Huang F, Bazan GC, Heeger AJ, Cao Y. *Energy Environ Sci*, 2013, 6: 3022–3034
41 Lee JK, Ma WL, Brabec CJ, Yuen J, Moon JS, Kim JY, Lee K, Bazan GC, Heeger AJ. *J Am Chem Soc*, 2008, 130: 3619–3623
42 Nguyen TL, Choi H, Ko SJ, Uddin MA, Walker B, Yum S, Jeong JE, Yun MH, Shin TJ, Hwang S, Kim JY, Woo HY. *Energy Environ Sci*, 2014, 7: 3040–3051
43 Guo X, Cui C, Zhang M, Huo L, Huang Y, Hou J, Li Y. *Energy Environ Sci*, 2012, 5: 7943–7949
44 Yao Y, Hou J, Xu Z, Li G, Yang Y. *Adv Funct Mater*, 2008, 18: 1783–1789
45 Wu JL, Chen FC, Hsiao YS, Chien FC, Chen P, Kuo CH, Huang MH, Hsu CS. *ACS Nano*, 2011, 5: 959–967
46 Ma W, Yang C, Gong X, Lee K, Heeger AJ. *Adv Funct Mater*, 2005, 15: 1617–1622
47 Li S, Yan J, Li CZ, Liu F, Shi M, Chen H, Russell TP. *J Mater Chem A*, 2016, 4: 3777–3783
48 Hardin BE, Snaith HJ, Mcgehee MD. *Nat Photon*, 2012, 6: 162–169
49 Jørgensen M, Norrman K, Krebs FC. *Sol Energ Mat Sol Cell*, 2008, 92: 686–714
50 Cheng P, Zhan X. *Chem Soc Rev*, 2016, 45: 2544–2582